Current Trends in Biotechnology and Pharmacy
Vol. 19(1) 2144-2158, January 2025, ISSN 0973-8916 (Print), 2230-7303 (Online)
DOI: 10.5530/ctbp.2025.1.4

Molecular Modelling, Hirshfeld Surface Analysis, Molecular Docking and Therapeutic Potential of Phenothiazine Derived Quinizarin

Shiny P. Laila[a], Vidya V. G.[a], Sherin G. Thomas[a], Arunkumar B[b], Viju Kumar V. G.[a]*

[a] Department of Chemistry, University College, Thiruvananthapuram, Kerala, 695034, India
[b] Department of Computational Biology and Bioinformatics, University of Kerala, Thiruvananthapuram, Kerala,695034, India

***Corresponding author:** *viju@universitycollege.ac.in

Abstract

Phenothiazine derivative synthesized from hydroxy anthraquinone, characterized by X-ray crystallography, spectroscopic, Hirshfeld surface, DFT studies and molecular docking investigation intent to ascertain its anti-cancer activity. The title compound 7-hydroxy-8-H-naptho[2,3-α]phenothiazine-8,13(14H)-dione crystallizes in orthorhombic lattice. UV-VIS, IR, NMR and mass spectrometric data were employed for characterization. Computational chemistry studies are conducted to further detail its geometrical and spectroscopic characteristics performed with unrestricted DFT method at of B3LYP/ 6-311+G (d, p) level and a comparison between the experimental and simulation results was performed. Non-covalent interactions primarily H-bonding and π-π stacking close contacts were observed at intermolecular levels. Small HOMO-LUMO energy gap of 2.2902 eV, shows the stability of molecule and effectiveness towards charge transfer interactions. Furthermore, MEP is used for predicting reactive sites. Based on Hirshfeld surface analysis, there is evidence for a wide range of interactions and a significant contribution from several non-covalent interactions to crystal packing. The bio-viability study was done using pre ADMET tool. The study elaborates the antitumor activity employing *in silico* molecular docking studies using the protein over-expressed in lymphoma cell lines namely p53 and BCL2 and when compared with standard drug doxorubicin revealed promising results. The study's results may inspire to develop more potent derivatives and similar scaffolds for cancer treatment and to explore phenothiazine's role in fields of material science, photochemistry, and catalysis, that can be analyzed from its structural and electronic properties. Hirshfeld surface analysis sheds light on the role of non-covalent interactions in crystal packing, influencing the compound's solid-state properties.

Keywords: hydroxyanthraquinone, phenothiazine, quinizarin, ADMET, DFT

Introduction

The anthracycline drugs comprise a number of chemotherapy medications commonly employed for the treatment of cancer and are popular for their potent anti-tumor activity and have been widely used for several decades. It works by inhibiting DNA replication and interfering with the function of topoisomerase enzymes, which are essential for DNA repair Studies on quinone compounds revealed that

anthraquinone ring when fused with oxazine moiety resembles that of anthracyclines, and exhibits various biological activity, involving a reduction in multidrug resistance [1]. Phenothiazines are related to oxazine in such a way that both came under the class of heterocyclic compounds which exhibits diversified pharmacological property in which the oxygen atom in the oxazine ring is replaced by sulphur atom which is an isostere of oxygen that forms the phenothiazine ring. These compounds can show varied biological activities like antimicrobial, antitumor, anticancer, and anti-inflammatory properties. It is believed that the diverse biological activity of phenothiazines is due to the presence of a folded axis along sulphur and nitrogen-containing heterocyclic ring. The reports on the bioactivity of DAQ are very few and less likely to be bioactive so an attempt was made to modify the structure of 1,4-dihydroxy anthraquinone by coupling reaction. Various amino and acetyl derivatives of anthraquinone have been reported [2]. There are several reports related to phenothiazine derivative of hydroxy benzoquinones and naphthaquinones, but the phenothiazine derivatives synthesized from hydroxy anthraquinone with C=O group in the 9 and 10 positions are very rare.

Cancer is caused mainly by the uncontrolled growth of cells or through different mutations which block the normal defenses that protect against unnatural growth. High levels of expression of p53 were found in many cancers so p53 was originally believed to be an oncogene [3,4]. The p53 protein is a phosphoprotein made of 393 amino acids and about 50% of all human tumors contain p53 mutants [5]. Though p53 is a tumor suppressor gene that shows a key role in the protection of our body from cancer. Mutated p53 could allow abnormal cells to proliferate, resulting in malignancy. Protein p53 gets mutated by the error caused due to placing an incorrect amino acid at a point in the protein chain. Thus, the normal functions of it will be blocked thereby, it is unable to repair the damaged cell. The work published by Zhen W *et al.,* [6] about the p53 protein state that synthetic drugs identified was selectively used to kill mutant p53-containing cancer cells and are very much helpful for chemoprevention. The certain synthetic drug can eliminate mutant p53-containing cancer-prone cells, at their early stage of carcinogenesis but one of the main adverse effects of drugs against mutated p53 is, normal cells containing non-mutated p53 will also be get destroyed. If the cell has other mutations, then that also causes uncontrolled growth which leads to the formation of the tumor. To prevent cell proliferation and to reduce genotoxic stress thereby maintaining genome integrity, tumor suppressor drugs are essential. The family of BCL2 protein consists of mainly 3 subgroups; BCL-2(anti-apoptotic/pro-survival proteins), BAX and Bak (pro-apoptotic proteins), BAD and BID (pro-apoptotic BH3-only proteins) [7]. Over-expression of the BCL2 gene is involved in cancer development. A large number of B-cell leukemias and lymphomas have the BCL2 gene transferred to a different chromosome. In this way, the BCL2 protein is produced in larger amounts, which may keep cancer cells alive. Thus it is found as a protein target within the breakpoint region of the t(14;18) translocation carried by persons with the follicular variant of B-cell lymphoma. The overexpression of BCL-2 can be found in 80% of B-cell Lymphomas. It is one of the key anti-cancer targets, which is chosen in the present study. One of the major roles of BCL-2 is it represses apoptosis by blocking the release of *cytochrome* complex from the mitochondria.

Owing to its multifunctional properties, this investigation focuses on the synthesis of an o-amino thiophenol derivative of anthraquinone. 1,4-dihydroxy anthraquinone (DAQ), also known as quinizarin, is a dye containing anthraquinone moiety. The interaction of the pharmacophoric substituent, via interaction of the multicyclic ring system improves the lipophilic character and allows the penetration of molecule into the biological membranes. From the study it has been revealed that the formation of

the phenothiazine core is a very potent pharmacophoric moiety which can be a rich source of desirable biological activities. In the present work the in silico biological activity was studied using iGEMDOCK software. Predicted poses of protein and ligand can be further understood from the post-analyzing tag. This can guide the biological researchers to explore better binding sites and interacting aminoacid. It was reported by Hamda M *et al.,* [8] 1996 that p53 mutations are associated with lymphoma. The apoptosis of cancer cells could be achieved by inhibition of this protein. In the present work, the synthetic derivative of hydroxyquinone and the standard drug doxorubicin was taken as the ligands and it is then docked with the targeted proteins. Though numerous in vitro methods are available to predict the absorption, distribution, metabolism and toxicity studies, all are time consuming so it is a common trend to predict and determine the toxicity and the ADME properties using different soft wares like SWISS ADME, preADMET etc. This the method to identify the effectiveness of a molecule to reach its target site. In the present work preADMET is used for predicting the various ADME parameters and Toxicity properties. The present study also investigates the electronic structure of the title compound, its quantum computational studies and supramolecular non-covalent contacts present in the crystal structure.

Materials and M ethods

Synthesis of 7-hydroxy-14-H-naptho[2,3-α] phenothiazine-8,13-dione (HNPD)

Quinizarin, o-aminothiophenol, and iodobenzene diacetate were purchased from Merck and used as such. All the solvents used for synthesis and purification were double distilled and dried using anhydrous calcium sulphate. A pre-coated aluminum plate of silica gel 60F 254 plates (0.25mm) was used for TLC. Column Chromatography is performed using silica gel of mesh size 100-200.

The derivative HNPD was synthesized as reported [9]. For the synthesis, 0.024 g of DAQ was dissolved in 20 ml of dichloromethane and a solution of 0.2 ml of o-aminothiophenol dissolved in 5 mL dichloromethane is added followed by the addition of a catalytic quantity of iodobenzenediacetate (IDA) and is shown in Scheme 1. The mixture is refluxed under a nitrogen atmosphere for 5 hours. The progress of the reaction was ascertained by TLC. After distilling CH_2Cl_2, the crude product is then washed with dil. HCl and neutralized with $NaHCO_3$ solution, extracted with ethyl acetate. The water content of the extract was removed by the addition of anhydrous sodium sulphate. precipitate was subjected to column chromatography by gradient elution method, using petroleum ether and ethyl acetate (60:80). The required product was eluted using pet ether: ethyl acetate in the ratio 8:2. Product was obtained as dark blue precipitate (55% yield). It was recrystallized by vapor deposition method using a mixture of CH_2Cl_2 and methanol, in which the product was highly soluble in CH_2Cl_2 and partially soluble in methanol. Thus obtained a dark blue colored needle-like crystals.

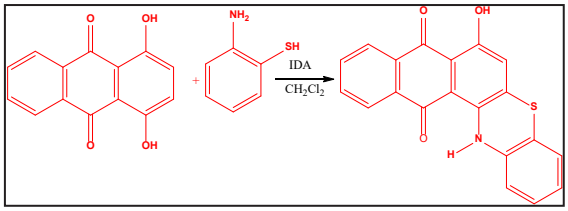

Scheme 1. Synthesis of HNDP

Spectroscopic analysis

Infrared spectra were recorded on a Shimadzu IR Prestige-21 FTIR spectrometer using KBr pellets. Proton NMR was taken in Bruker advanced spectrometer of 500 MHz with $CDCl_3$ as the solvent. The mass spectrum was recorded in the Shimadzu GCMS spectrometer. UV-Vis spectrum was recorded in Shimadzu-UV-3600. Single crystal X-ray diffraction was performed in Bruker AXS Kappa Apex2 CCD diffractometer with Mo Kα radiation using ωϕ scan mode at ambient temperature. The program SAINT/XPREP was used for data reduction and APEX2/SAINT for cell refinement. The

Current Trends in Biotechnology and Pharmacy
Vol. 19(1) 2144-2158, January 2025, ISSN 0973-8916 (Print), 2230-7303 (Online)
DOI: 10.5530/ctbp.2025.1.4

structure was solved using SIR 92 and refinement was carried out by full-matrix least square of F^2 using SHELXL-97.

Quantum computational investigations and molecular docking

Density Functional Theory calculations are aimed to study electronic structure of molecules using *Gaussian 16W* software with B3LYP/6-311+G(d,p) level of theory and graphical representations are generated using *GaussView 6.1*. Corresponding Molecular graphics are generated by MERCURY and PLATON. *Crystal explorer 21* sketches and quantitatively express interactions in molecular crystal, through Hirshfeld surfaces and corresponding 2D- fingerprint plots. It can be used to calculate and visualize various properties of crystals, such as electron density, electrostatic potential and electron localization function. It also analyzes intermolecular interactions and chemical bonding in crystals. The B3LYP/6-311G (d,p) level of theory was used for generating energy framework in crystal fabrication.

iGEMDOCK is a computational software that works on empirical scoring functions that integrate; docking, post-analysis, visualization, and screening. iGEMDOCK is used for finding the interactions of the compounds with the targeted protein molecules BCL2 and p53. The predicted pose generated after the docking procedure is visualized and then analyzed by post-analysis tool Discovery Studio visualizer [10,11]. iGEMDOCK provides the post-analysis tools using k-means and hierarchical clustering methods based on the docked poses and atomic compositions. The ADMET results were obtained from PreADMET tool [12, 13].

To start a docking/screening procedure, two files are to be prepared, a protein structure file and a ligand file. The protein structure file can be obtained from a protein data bank. Selection and identification of a drug target or receptor is the first step involved in the drug-designing process. Different computational tools are being used to find out excellent drug targets. For a drug target to be ideal, it must be linked closely to the selected human disease. In the present investigation, BCL2 and mutated p53 were taken as the drug targets.

Results and Discussion

Commentary on crystal structure

The crystal structure was reported by our research group earlier. [9]. The space group of phenothiazine derivative HNPD is P2(1)2(1)2(1) and crystallizes in orthorombic space lattice. The ORTEP diagram of the molecule is given (Fig.1). C-O bond distance C19-O1 1.249 Å and C6-O21.242 Å, indicated that the molecule existed in the keto form. From SCXRD analysis, bond distance of C8-N1 and C9-N1 were 1.365 Å and 1.393 Å respectively which was found to be greater than 1.28 Å and this confirmed the presence of C-N bond rather than C=N bond. The bond angle of C9-N1-C8 was found to be 128.94°. The bond angle between C15-S1-C14 was observed at 103.6 Å which revealed that the S atom has taken part in the cyclisation leading to the formation of heterocyclic phenothiazine ring system [14].

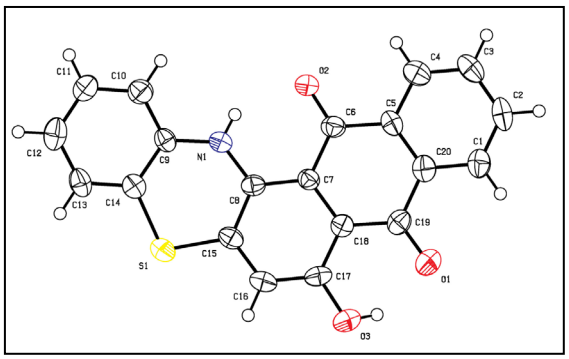

Fig. 1. Crystal structure of HNPD

Prediction of ADMET Properties

Different biological parameters like blood-brain barrier permeability (BBB), solubility, various inhibitions, skin permeability, plasma protein binding affinity, partitions coefficient, and different toxicity study to find the mutagenic activity, liver toxicity, etc. were determined using

preADMET software. All the parameters were then compared with the sample compound and the standard drug Doxorubicin. HNPD and Doxorubicin got a human intestinal absorption ability of 95.91%, 56.84%. There is CYP2C9 and CYP3A4 enzyme inhibition observed with HNPD while no inhibitory activity on CYP2D6, which is essential for metabolism of many drugs and toxic chemicals. Doxorubicin inhibits the enzymes CYP2C9, CYP2D6 but a substrate of CYP3A4.

The MDCK (Madin Darby Canine Kidney Cell line) evaluation, which is helpful for the rapid screening of cell permeability gave a low value of 16.10 for HNPD which means its diffusivity through the cell membrane is low. A value of 1.02 has been observed for the standard drug doxorubicin, means good diffusivity through the cell membrane. The HNPD compounds can act as an inhibitor of Pgp (glycoprotein) but doxorubicin has no Pgp(glycoprotein) inhibition. The solubility of HNPD in water is 0.001 but the standard drug doxorubicin has got high water solubility (8.34). The permeability though the skin is the next important parameter. The skin permeability value is -3.624 which means the HNPD compound provides good absorption via skin. The doxorubicin has also good value (-4.737). The more the negative value of permeability, lower will be the solubility. The toxicity prediction of all HNPD compounds were conducted by Ames test, and from the results HNPD is mutagen exhibiting carcinogenic activity in rat and mouse model. The doxorubicin is non mutagenic. The negative values for TA1535_10RLI indicates non mutagenic while TA100_NA is positive for HNPD compound. The negative values for doxorubicin which means non mutagenic. The hERG (The Human Ether-a-go-go-Related Gene) analysis when done using the PreADMET software displays high risk for HNPD but was ambiguous in the case of standard drug doxorubicin. All the data of ADME and toxicity are given in Table 1 and Table 2 respectively.

Table 1. ADME-parameters

ID For ADME	Values	
	HNPD	DOXO
BBB	1.02598	0.0355281
Buffer_solubility_mg_L	0.196846	3963.51
$CaCO_3$	3.41067	17.7263
CYP_2C19_inhibition	Non	Inhibitor
CYP_2C9_inhibition	Non	Inhibitor
CYP_2D6_substrate	Non	Non
CYP_3A4_inhibition	Non	Weakly
CYP_3A4_substrate	Weakly	Inhibitor
HIA	95.910386	Weakly
MDCK	16.1011	56.840587
Pgp_inhibition	Inhibitor	1.0236
Plasma_Protein_Binding	97.123298	Non
Pure_water_solubility_mg_L	0.0014759	31.160238
Skin_Permeability	3.62419	8.34623
SKlogD_value	4.379130	4.73786
SKlogP_value	4.379130	0.314800
SKlogS_buffer	-6.244160	-2.137140
SKlogS_pure	8.369230	-4.813730

Table 2. Toxicity parameters

ID For Toxicity	Values	
	DOXO	HNPD
algae_at	0.0118035	0.0202937
Ames_test	non-mutagen	mutagen
Carcino_Mouse	negative	negative
Carcino_Rat	negative	negative
daphnia_at	0.553548	0.0092121
hERG_inhibition	ambiguous	high_risk
medaka_at	0.704316	0.000247842
minnow_at	0.511881	0.000340659
TA100_10R	negative	positive
TA100_NA LI	negative	positive
TA1535_10RLI	negative	positive
TA1535_NA	negative	positive

Current Trends in Biotechnology and Pharmacy
Vol. 19(1) 2144-2158, January 2025, ISSN 0973-8916 (Print), 2230-7303 (Online)
DOI: 10.5530/ctbp.2025.1.4

Computational chemistry studies

Geometry optimization

The optimized molecular geometry of HNPD was reported using B3LYP/6-311+G(d,p) and is shown in fig.2. The C28-O32 bond length is found to be 1.2488 Å close to actual value of 1.249 Å. The newly formed bonds between C13-N15 & C21-S30 are found to have an optimized bond lengths of 1.3901 Å & 1.7701 Å which coincides with 1.393 Å & 1.767 Å respectively in crystal structure. The bond lengths C25-O26 & C10-O33 are found be 1.3336 & 1.2437 that agrees to values 1.329 Å & 1.242 Å. The other optimized bond lengths N15-C12, C29-C9, C27-C28, C10-C9, C23-S30, C25-C27, C23-C12, C10-C11 and C28-C29 are 1.3698, 1.4053, 1.4542, 1.485, 1.7707, 1.4055, 1.4313, 1.4664 Å and 1.476 that concede to speculative results of 1.365, 1.402, 1.436, 1.476, 1.747, 1.435, 1.435, 1.462 &1.438 Å respectively. All the optimized bond angles are exploratory to crystal structure values. The bond angle ranges from 117.8^0- 122.7^0 throughout the molecule, except C21-S30-C23, C12-N15-C36, C24-C23-S30, C25-O26-H35 and C12-N15-C13 bond angles are 103.2^0, 112.6^0, 116.4^0, 106.0^0 and 128.4^0 respectively. The newly formed bond angles show maximum deviation of 103.2^0 and 128.4^0. A tremendous amount of agreement exists between experimental and theoretical values.

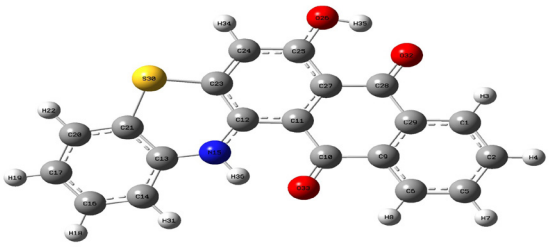

Fig. 2. Optimized geometry of HNPD

As shown in the simulated FT-IR spectrum, -OH and -NH stretching frequencies are detected peak at 3230 cm-1 and 3104 cm^{-1} along with aromatic C-H at 3066cm^{-1}. A strong peak at 1609 $cm^{-1}$is due to >C=O group. The band at 1262cm-1 and 1350cm^{-1} are due to the C-N and C-S stretching frequencies. The C-S-C stretching frequency was seen at 734cm^{-1}. The experimental IR spectrum gave peaks at 1350 cm^{-1} which corresponds to C-N stretching. The C-S stretching frequency was observed at 1262 $cm^{-1}$and stretching frequency due to C-S-C gave an absorption in the finger print region 744 cm^{-1}. Aromatic C-H stretch was observed at 3066 cm^{-1}. N-H and O-H functional groups gave absorption bands in the range 3452-3200 cm^{-1}. These values are in tune with the simulated values.

In the UV-Visible spectrum, the absorption maxima λ_{max} in $CHCl_3$ were observed at 692 nm, 641 nm and 597 nm. A bathochromic shift which was observed in HNPD indicated the intra molecular charge transfer transition (ICT) between electron donor and electron acceptor moiety. We computed the UV-Visible spectrum using TD-DFT method with maximum absorbance at 604 nm and the theoretically calculated absorption wavelength of the title compound shows variation as it is calculated for a single molecule in vacuum and not in solid state.

The structure was further confirmed by NMR and mass spectral analysis. The ^1H NMR spectrum of HNPD in $CDCl_3$ gave peaks at δ 6.717, δ 6.801, δ 6.816, δ 6.833, δ 6.8796, δ 8.967, δ 7.052, δ 7.071, δ 7.800 which corresponded to the aromatic protons. -NH and -OH protons are observed at δ 12.698 and δ 14.202 respectively. The ^{13}C NMR in $CDCl_3$ revealed the presence of different aromatic carbon environment at δ 115.23, δ 115.93, δ 117.26, δ 118.25, δ 102.83, δ 123.81, δ 125.77, δ 126.35, δ 126.84, δ 127.08, δ 128.32, δ 131.60, δ 133.28, δ 133.88, δ 134.51 and δ 136.83. The -C=O groups of anthraquinone moiety were obtained at δ 180.90 and δ 181.25. The presence of one hydroxyl group was indicated by the presence of a peak in the region δ 160.60. In the mass spectrum of HNPD the molecular ion peak was observed at 345(100%) which was the base peak, M+1 peak at 346 and (M+OH) at 328.

Current Trends in Biotechnology and Pharmacy
Vol. 19(1) 2144-2158, January 2025, ISSN 0973-8916 (Print), 2230-7303 (Online)
DOI: 10.5530/ctbp.2025.1.4

Thermodynamic parameters of HNPD obtained through DFT studies are given in Table 3.

Table 3. Thermodynamic properties of HNPD

Thermal energy	175.053845 kcal/mol
Heat Capacity (Cv)	74.263 cal/mol-kelvin
Entropy (S)	137.78 cal/mol-kelvin
Electronic Energy (EE)	-908452.43665 kcal/mol
Zero-point Energy Correction	163.703452 kcal/mol
Enthalpy	175.64621 kcal/mol
Free Energy	134.567553 kcal/mol
EE + Zero-point Energy	-908288.71939 kcal/mol
EE + Thermal Energy Correction	-908277.36147 kcal/mol
EE + Thermal Enthalpy Correction	-908276.79671 kcal/mol
EE + Thermal Free Energy Correction	-908317.83584 kcal/mol

Mulliken population analysis

In quantum chemical calculations, Mulliken charge calculations have a significant role because they affect electronic structures, dipole moments, polarization, and other properties of molecules. By studying each atom's electronic population, Mulliken charges can be determined. The total atomic charges of HNPD obtained by Mulliken population analysis with 6-311+G(d,p) basis set is given in fig. 3. The Mulliken atomic charge of C_{21} atom of phenyl group attached to Sulphur has highest positive value of 1.060576 and is acidic in nature. An increased electron density is seen in carbon atoms C_2, C_5, C_{10}, C_{12}, C_{13}, C_{14}, C_{16}, C_{17}, C_{20}, C_{25}, C_{26} and C_{28} that has values -0.3647, -0.4353, -0.1321, -0.2387, -0.532, -0.2092, -0.3735, -0.0585, -0.3894, -0.3017, -0.3106, -0.120. All other carbon atoms are positively charged. Here in HNPD all eleven hydrogen atoms shows positive charge, among which the highest positive charge is on hydrogen atom attached to nitrogen atom, H_{36} with value 0.3406 and oxygen, H_{35} having value 0.3348. The nitrogen atom has a net charge of 0.0297. All the three oxygen atoms are negatively charged O_{26}, O_{32}, O_{33} with -0.3106, -0.322 and -0.2879 values. The Sulphur atom is negative and has a value of -0.5083 value. The electrophilic substitution can happen on Sulphur rather than on nitrogen.

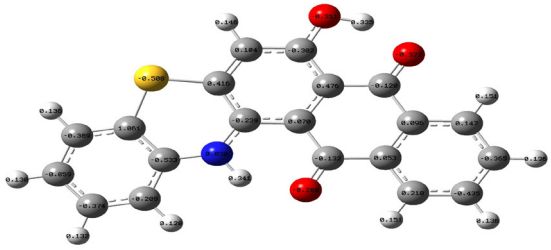

Fig. 3. Mulliken charges of HNPD

Molecular electrostatic potential (MEP)

The MEP was evaluated using DFT to investigate the reactive sites of HNPD. The distribution of electrostatic charge is illustrated in three dimensions by molecular electrostatic potential energy maps. Fundamentally, electrostatic potential energy computes the strength of nearby charges, nuclei, and electrons. The MEP can be used to predict chemical reactions by giving insight into the active sites of attack by electrophile or nucleophile [15]. Hydrogen bond interactions and behavior towards charged species can be sketched with the help of MEP. Interactions towards various receptors like proteins, enzymes can be recognized by MEP plots as shown (Fig. 4).

Those regions with attractive potential are red, while those with repulsive potential are blue. So, the red region holding negative potential depicts the minimum electrostatic potential. In the present system the alcoholic oxygen and two carbonyl oxygen atoms act as site for electrophilic attack. The blue regions can receive nucleophile, hydrogen atoms on aromatic rings in present case. To generate and display

difference in electron density, the difference in electron density between the first excited state from total CI density matrix and the ground state based on total SCF density is mapped to SCF density and is shown in Fig.5. The blue contour maps positive values of difference density where excited state density is larger than ground state density and red contour denotes the opposite. In present system, the electron density flows from the left side to anthraquinone ring as the transition happens from ground state to excited state.

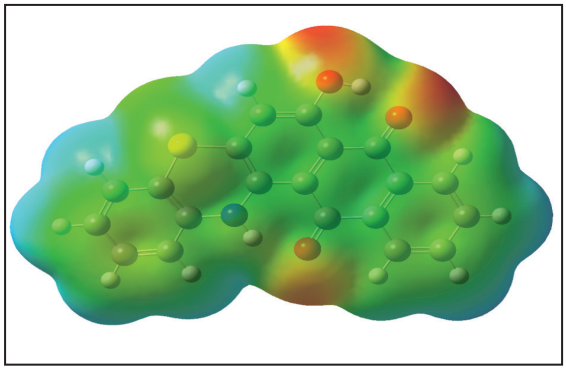

Fig.4. Plot of ESP on electron density surface

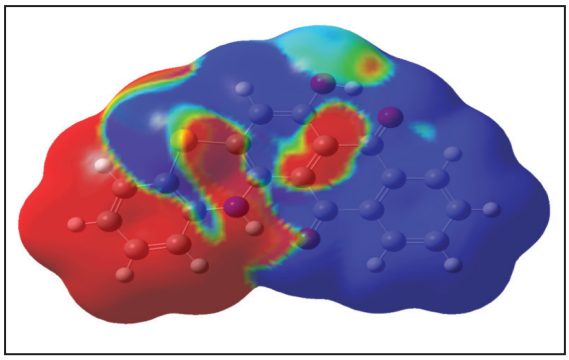

Fig. 5. MEP plot of difference of SCF and CI into ground state

Frontier molecular orbital analysis (FMO)

Analyzing FMOs can provide insight into organic compounds' optical and electronic properties. The properties of molecular orbitals, including energy, help us predict the most reactive site in two-electron systems and also describe many different types of reactions that occur in conjugated systems. To evaluate the chemical reactivity of molecules, it is useful to know how HOMO and LUMO interact, as well as their properties, such as their energy. As electrons transfer from the LUMO to the HOMO during molecular interactions, the LUMO's energy correlates with electron affinity, and the HOMO's energy corresponds to the ionization potential (IP). HOMO-LUMO energy gaps are useful for determining molecular electrical transport properties and explaining charge transfer interactions within molecules. FMO of HNPD is shown in fig. 6.

In HNPD the electron density is localized on phenyl ring on C_{25}, C_{27}, C_{28} Sulphur and Nitrogen atom and in HOMO-1 it is seen entirely on phenyl ring alone. In HOMO and HOMO+1, the third hexagon of anthracene ring lacks electron density. On moving from HOMO to LUMO the electron density shifts towards anthracene ring, where phenyl ring has nil electron density. In LUMO+1 the electron density occurs throughout the whole molecule. There is an energy gap of 2.2902 eV in this system [16]. Structure's firmness is highlighted by the energy gap. In contrast to a high HOMO-LUMO gap, a low HOMO-LUMO gap indicates a more stable molecule with higher charge transfer. Especially in conjugated and soft molecules, a small energy gap can cause low excitation energies and high levels of intramolecular charge transfer.

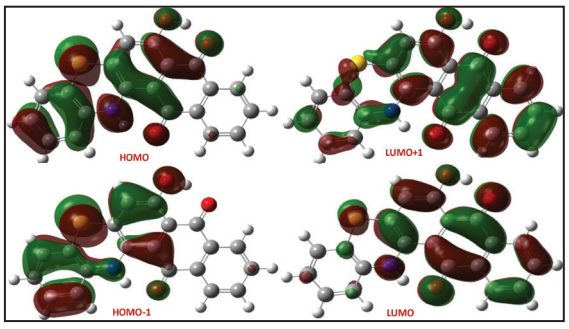

Fig. 6. HOMO and LUMO of HNPD

Hirshfeld surface (HS) analysis

Hirshfeld surface analysis is a valuable tool in computational chemistry that allows for

Current Trends in Biotechnology and Pharmacy
Vol. 19(1) 2144-2158, January 2025, ISSN 0973-8916 (Print), 2230-7303 (Online)
DOI: 10.5530/ctbp.2025.1.4

the visualization and quantification of intermolecular interactions with a detailed emphasis on the spatial distribution and nature of these interactions, aiding in the interpretation of molecular behavior and properties in crystal architecture. The analysis is based on the concept of the Hirshfeld surface, which is constructed by mapping the density distribution of one molecule onto a surface surrounding another molecule or group of molecules. This surface represents the region of space where the interacting molecule or group of molecules influence the electron density of the molecule of interest.

The following expression generates a Hirshfeld surface formed by the continuous scalar function on 0.5 isosurface.

$$w_A(r) = \rho_{promol}(r) / \rho_{procrystal}(r) = \frac{\sum_{A \in molecule} \rho_A(r)}{\sum_{C \in crystal} \rho_C(r)}$$

Where $w_A(r) = \rho_{promol}(r) / \rho_{procrystal}(r) \rho_A(r)$ are weight function, promolecule electron density, procrystal electron density and atomic electron density respectively.

The *Crystalexplorer 21* program maps the normalized contact distance depicted by d_{norm} in terms of the closest nucleus externally and internally to the Hirshfeld surface which is d_e and d_i. The blue shade denotes atoms in close contacts with longer vdW than the red patched regions, whereas the red spots denote the opposite. In cases where distances are approximately vdW, white is predominant.

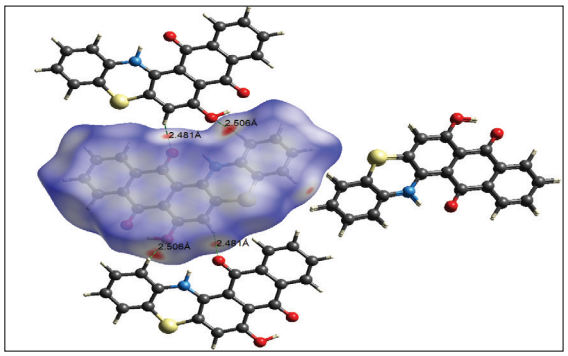

Fig. 7. d_{norm} mapped on Hirshfeld surface showing the intermolecular contacts

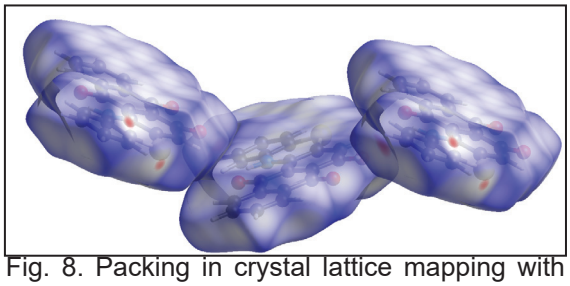

Fig. 8. Packing in crystal lattice mapping with Hirshfeld surface

Bright red spots in Fig.7 are due to C-H--O- interaction at an internuclear distance of 2.49±0.01Å. these major interactions held the molecules in XY plane as shown in Fig.8. The aromatic rings are spatially arranged through parallel displaced π-π stacking interactions where all the carbon atoms and heteroatoms of two layers keeps the exact interacting distance. The average distance between two adjacent layers is 3.806 Å (Fig. 10). Ideal distance between two aromatic platform keeps a centroid-centroid distance of ~3.5 Å [17] and in present case its slightly higher due to higher Van der Waals radius of sulphur and oxygen atoms of the ring system and forms a see-saw motif (Fig.9).

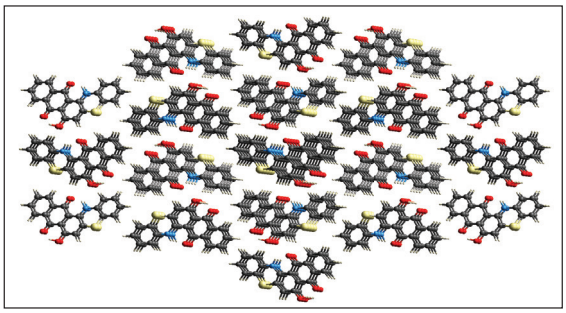

Fig. 9. The ring system forming a see-saw motif

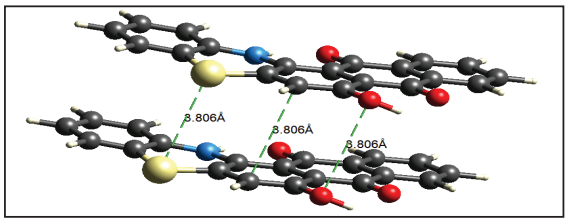

Fig. 10. Crystal packing showing molecular array with π-π stacking interactions

Current Trends in Biotechnology and Pharmacy
Vol. 19(1) 2144-2158, January 2025, ISSN 0973-8916 (Print), 2230-7303 (Online)
DOI: 10.5530/ctbp.2025.1.4

It is possible to better understand the interactions occurring within a crystal by using two-dimensional fingerprint plots, shown in Fig.11, associated with the Hirshfeld surface. A molecule's immediate surroundings influence 2D fingerprint plots, and filtering is done by the type of element and surface area, which enumerates close contacts between atoms inside and outside the HS surface, shown in fig.12 [18]. H—H close contacts are characterized by blunt peak which is positioned at $d_i+d_e \approx 2.4$ Å. Remarkable and well-defined O—H/H—O interactions are observed as sharp peaks at $d_i+d_e \approx 2.8$ Å which spans around 17.9 % of the total HS area. The pale green region falls diagonally in the fingerprint plot of C--C contacts at $d_i \cong d_e$ □ 1.7 Å reinforces the existence of characteristic π-π stacking, comprising 19.8 % of HS area [19]. C--H and S--H close contacts are also prominent which appears as two sharp wings comprising 12.3 and 5.2 % respectively of total area.

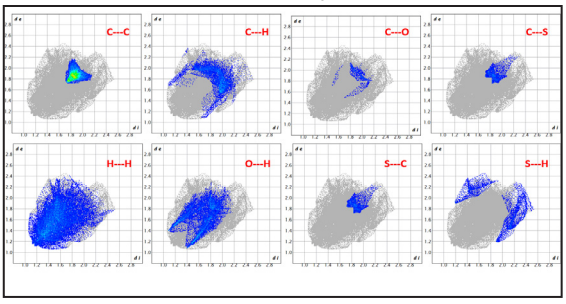

Fig. 11. Decomposed 2-D fingerprint plots of HNPD

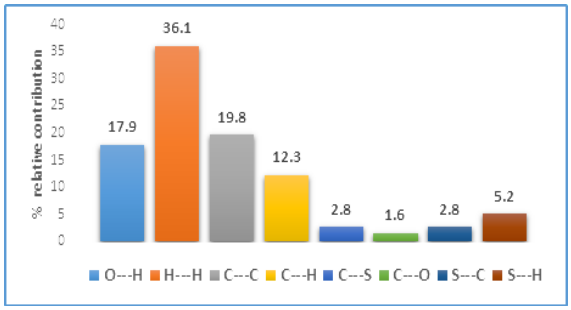

Fig. 12. Relative contributions of major close contacts in crystal lattice

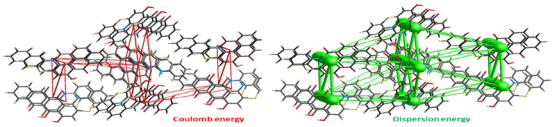

Fig. 13. Energy frameworks in 3D molecular packing (Energies <10 kJ mol^{-1} have been discarded)

For fabricating energy frameworks, single point wavefunctions with B3LYP functional incorporating 6-31G(d,p) basis set in order to compute interaction energies inside a cluster of molecules [Fig. 13]. Total energies, benchmarked for B3LYP/6-31G(d,p) energy model and scaled appropriately, are provided as the sum of four principal energy components namely electrostatic (E_{ele}), polarization (E_{pol}), dispersion (E_{disp}) and exchange-repulsion (E_{rep}) (Table). For simplification, close contacts with energies below 10 kcal/mol have been discarded. The distinct 3D topology with respect to b-axis., give different infrastructure for coulomb energy and dispersion energy. Stacked layers are maneuvered into a hexagon motif and larger tubes of dispersion energy fame work passed between NH and CO groups which seems to run along with the crystallographic c-axis. The packing of crystal lattice of the title complex is majorly driven by the dispersion energy component.

Table 4. Interaction energies generated within a cluster of radius 3.8 Å

N	Symop	R	E_{-ele}	E_{-pol}	E_{-dis}	E_{-rep}	E_{-tot}
2	x, y, z	3.81	-9.2	-2.7	-111.9	54.8	-67.5
2	-x, y+1/2, -z+1/2	7.86	-8.9	-2.3	-22.6	14.5	-19.3
2	x+1/2, -y+1/2, -z	13.13	-3.3	-1.0	-11.8	7.3	-8.7
2	-x+1/2, -y, z+1/2	14.04	-1.5	-0.7	-9.2	4.5	-6.6
2	x+1/2, -y+1/2, -z	12.66	-6.9	-1.6	-10.0	3.7	-14.1
2	-x, y+1/2, -z+1/2	7.77	-6.3	-2.4	-22.2	8.1	-21.5
2	-x+1/2, -y, z+1/2	14.50	2.3	-0.9	-8.0	3.7	-2.5

'N' corresponds to the number of molecules with centroid-to centroid distance 'R'.
Energy values in kJ mol^{-1} and R in Å.

Molecular docking studies

iGEMDOCK (integrated GEMDOCK) is a molecular docking software used for predicting the binding modes and affinities of small

molecules with protein targets. It is specifically designed for high-throughput virtual screening and drug discovery applications. iGEMDOCK employs a combination of a genetic algorithm and an empirical scoring function to perform molecular docking simulations. The software takes a protein structure and a small molecule ligand as input and generates a set of possible binding conformations. These conformations are then scored using an empirical scoring function that evaluates the intermolecular interactions between the protein and the ligand. The genetic algorithm is used to optimize the conformational search and exploration of the ligand binding space. The tool is used to predict the affinity of the molecule towards two proteins BCL2 and p53 which are the mutated proteins responsible for the cancer in lymph nodes. Both the proteins were selected from the Protein Data bank with PDB id 2X0W (p53 protein) and 4LVT (BCL2 protein). By preparing two files, the protein structure file, and Ligand file docking was performed using iGEMDOCK software, and the results obtained were expressed in terms of free energy. Both the standard drug and sample compound HNPD were subjected to computational studies and the results were compared. Discovery Studio Visualizer is used to sketch the docked poses and to shine light upon different types of interactions existing between the ligand and proteins [20].

The most frequently interacting amino acids with compounds of anthraquinone moiety were PRO, THR and LEU. The interactions of major amino acid residues present in p53 protein with ligands of a particular class having better docking affinity along with the docking pose of standard drug (Doxorubicin) is given below. Interactions of amino acids with ligands in the active site of mutated p53(2XOW) protein indicates that Hydrogen bonded interactions, pi-alkyl, pi-sigma and van der Waals interactions are dominant in the case of derivative while van der Waals and hydrogen bonded interactions are exist in Doxorubicin. Different types of interactions of p53 with the standard drug and HNPD are given. (Table 5) From the in-silico studies the interaction of amino acids with ligands in the active site of mutated BCl2(4LVT) protein with various amino acid residues indicate that the title compound is found to be higher than that of the standard drug Doxorubicin The derivative is found to possess all types of interactions like pi-sigma, pi-alkyl, Pi-Anion, Pi-Donor Hydrogen Bond, Pi-sulfur and van der Waals interactions while the standard drug Doxorubicin has got pi-alkyl interactions alone. (Table 6)

Table 5. Docked files of ligand and standard drug with 2X0W(p53)

Sl.No.	Ligand	Amino acid residues				
		van der Waals	Hydrogen bond	Pi-sigma	Pi-alkyl	Pi-donar hydrogen bond
1	HNPD	PROB153	GLYB:154 THRB:155 CYSB:220	PROB:151	PROB:222 VALB:147 PROB:223	THR B:150 GLU B:220
2	DOXO (STD)	THRB:230,155, 150 VALB:147 PROB:151, 223, 219 GLYB:154 GLUB:221 ARGB:202	CYSB:220	-	-	-

Current Trends in Biotechnology and Pharmacy
Vol. 19(1) 2144-2158, January 2025, ISSN 0973-8916 (Print), 2230-7303 (Online)
DOI: 10.5530/ctbp.2025.1.4

Table 6. Docked files of ligand and standard drug with 4LVT(BCL2)

Sl. No.	Ligand	Amino acid residues				
		van der Waals	Pi-Anion	Pi-Donor hydrogen bond	Pi-sulfur	Pi-Alkyl
1	HNPD	GLUB:133 ALAB:146 VALB:130 PHEB:150 GLUB:149 SERB:113	ASPB:108	TYR B:105	PHEB:109 PHEB:101	LEUB:134 VALB:134 METB:112
2	DOXO (STD)	-	-	ASPB:108	-	PHEB:150 ALAB:146 METB:112

Table 7. Docking parameters of proteins with title compound and standard drug

Docking score of p53 (pdb-2X0W)					
Sl. No.	Name	Energy	VDW	H bond	Electrostatic force
1	HNPD	-112.57	-100.62	-12.15	0
2	DOXO(STD)	-117.99	-100.08	-17.91	0
Docking score of BCL2 (pdb-4LVT)					
Sl. No.	Name	Energy	VDW	H bond	Electrostatic force
1	HNPD	-79.68	-54.65	-25.03	0
3	DOXO(STD)	-99.21	-68.43	-30.77	0

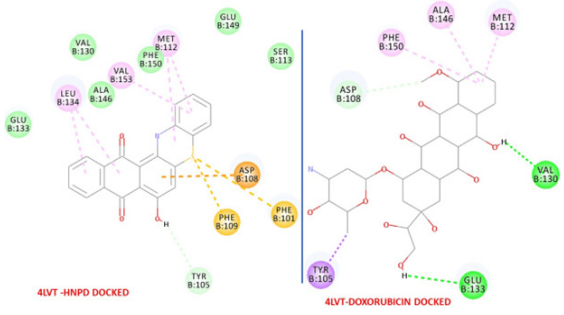

Fig. 11. 2D representation of ligands inside 4LVT receptor pocket

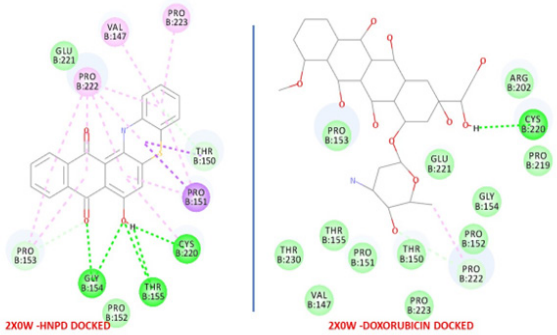

Fig. 12. 2D representation of ligands inside 2X0W receptor pocket

Potential as drug candidate of a molecule can be inferred from the ligand (drug)- protein interaction in terms of binding energy. The docked scores of the molecules are given in Table 7. Various interactions like van der Waals, Pi-alkyl, Pi-sigma and hydrogen bonded interactions were found to be exist between ligand and protein pocket. HNPD and standard drug Doxorubicin has got van der Waals and hydrogen bond interactions in common with p53 and all other interactions like Pi-sigma, pi-alkyl and pi-donor hydrogen bond is present only within HNPD that is all the latter interactions are absent. In the case of binding affinity towards BCL2 the standard drug Doxorubicin has got Pi-Donor Hydrogen Bond and Pi-alkyl interaction. The van der Waals, Pi-sulphur and Pi-alkyl interactions are dominant in the case of HNPD.

Conclusion

One of the most feared cancers is lymphoma, which spreads easily and is extremely deadly, but effective drugs are a few. The present investigation purports to synthesize an o-amino thiophenol derivative of anthraquinone with potent biological activity. The SCXRD data of 7-hydroxy-8-H-naptho[2,3-α]phenothiazine-8,13(14H)-dione suggests an orthorhombic lattice. UV-VIS, IR, NMR and mass spectrometric data were collected and analyzed and supports the formation of intended compound. A potential for drug candidate was assessed for its ADMET and toxicological properties to assess drug likeness and therapeutic efficacy. IR, UV-Visible, Mulliken charge analysis, geometry optimization and thermochemical investigation were performed with unrestricted DFT method at the level of B3LYP/6-311+G(d,p) and the results were in consistent with experimental data. Small HOMO-LUMO energy gap of 2.2902 eV of shows the stability and effectiveness of the title molecule to incorporate charge transfer interactions. Numerous non-covalent interactions have been revealed in crystal packing, according to Hirshfeld surface analysis. Aromatic rings are arranged spatially through π-π stacking interactions in which carbon atoms and heteroatoms of two layers maintain the exact same distance between them. Separating adjacent molecular layers require 3.806 Å internuclear distance. The predominant C---C, O--H and H--H close contacts comprise 73.8 % of the total HS area. An in silico inhibitory activity of HNPD on two over expressed protein in lymphoma namely p53and BCL2 were carried out using iGEMDOCK tool which gave comparable score with standard drug Doxorubicin. The bio-viability study of HNPD using preADMET software also gave a promising result. Thus, HNPD can be used as a lead molecule against Lymphoma. There are remarkable weak interactions involving hydrogen bonds and aromatic stacking close contacts that can be tuned with high selectivity which in turn are responsible for the enhanced pharmacological activity revealed through molecular docking studies.

Acknowledgment

The authors would like to express deep gratitude to the Department of Chemistry, University College Thiruvananthapuram for providing computational laboratory facility. We also thank Department of Computational Biology and Bioinformatics, Kriyavattom, Thiruvananthapuram for laboratory facility.

Declarations

Conflicts of interest

The authors do not have any conflict of interest.

Ethical Approval

Not applicable.

Funding

No funding recieved

Availability of data and materials

Data will be made available on request.

References

1. Dzieduszycka, B., Stefa_nska, M., Gawro

nska, M., Arciemiuk, E., Borowski, Synthesis of new polycyclic anthracenedione analogs with hetero- or carbocyclic ring(s) fused to the chromophore system, *Pol. J. Chem*., **81**, 2007, 535-546.

2. Supranee, S., Helen, H., Thapong, T., Nattaya, N., Nouri, N., Nongnuj, M., Overcoming doxorubicin-resistance in the NCI/ADR-RES model cancer cell line by novel anthracene-9,10-dione derivatives*, Bioorg. Med. Chem. Lett.,* **23**, 2013, 6156-6160.

3. Meek, D., Regulation of the p53 response and its relationship to cancer, *Biochem. J.,* **469(3)**, 2015, 325-46.

4. Muller, P., Vousden, K.H., p53 mutations in cancer, *Nature Cell Biology*. **15(1)**, 2013, 2-8.

5. Ling, B., Wei-Guo, Z., p53: Structure, Function and Therapeutic Applications, *J. Cancer Mol.,* **2(4)**, 2006. 141-153.

6. Zhen, W., Yi S., Targeting p53 for Novel Anticancer Therapy, *Transl Oncol.,* **3(1)**, 2010,1-12.

7. Blaineau, S. V., Aouacheria, A., BCL2DB: Moving "helix-bundled" BCL-2 family members to their database. *Apoptosis* **14**, 2009 923–925

8. Hamda, M., Fujiwara, T., Hizuta, A., Gochi, A., Naomoto,Y Takakura, N., Takahashi, K., Roth, J.A., Tanaka, N., Orita, K., The p53 gene is a potent determinant of chemosensitivity and radiosensitivity in gastric and colorectal cancers, *J. Cancer Res. Clin. Oncol.,* **122(6)**,1996, 360-365.

9. Shiny, P. L**.**, Annette, F., Arun, K. B, Vishnu, V. S., Rema, D. K., Archana, P. D., Thomas, O., Synthesis, Single Crystal Study, in silico Analysis, in vitro Anti-inflammatory and Anticancer Activities of 7-hydroxy-14H-naphtho[2,3- a]phenothiazine-8,13-dione*, Drug Delivery Letters*, **5(2)**, 2015, 140-150.

10. Priya, R.P., Indu, P.I., Sangeetha, K., Raja, R.S.R., discovery of a novel Binding trench in BMRF1 of Epstein BARR Virus an in silico approach, *Int J Pharm Pharm Sci.*, **6(1)**, 2014, 578-584

11. Kumar, A., Ram, T., Goel, B., Bansal, E., Srivastava, V.K., Synthesis and anti-inflammatory activity of some potential cyclic phenothiazines. *Boll. Chim*. *Farm,* **137**, 1988, 152-156.

12. Lipinski, C.A., Lambardo, F.M., Doming, B.W., Feeney, P.J., Experimental and computational approaches to estimate solubility and permeability in drug discovery and development settings, *Adv. Drug Delivery Rev.,* **46**, 2001, 3-26.

13. Daina, A., Michielin, O. & Zoete, V. SwissADME: a free web tool to evaluate pharmacokinetics, drug-likeness and medicinal chemistry friendliness of small molecules. Sci Rep 7, 42717 (2017)

14. Dandia, A., Sarawgi, P., Hursthouse M.B., Bingham, A.L., Elight M., Drake J.K., Ratnani R., Vibrational spectrostroscopic (FT-IR,FT-Raman) and quantum chemical calculations of 1-(5,5-dioxido-10H-Phenothiazine-10-yl)ethanone, *J. Chem. Res*., 2006, 445-448.

15. Anila Raj S., Vidya, V. G., Preethi V., Viju Kumar V. G., Single Crystal XRD and DFT investigation of 1,5-dimethyl-4-[(2-oxo-1,2-diphenylethylidene) amino]-2-phenyl-1,2-dihydro-3H-pyrazol-3-one. *Results in Chemistry*, **4,** 2022, 100665. 10.5267/j.ccl.2022.9.006

16. Abhijith, V. H., Vidya, V. G., Viju Kumar, V. G. DFT computations, Spectral investiga-

tions and Antimicrobial studies of Zn (II) complex with α-diketimine ligand. *Results in Chemistry*, **8(6)**, 2022 100420**.** https://doi.org/10.1016/j.rechem.2022.100420.

17. Leslie-Joana Riwar, Nils Trapp, Bernd Kuhn, and Francois Diederich, Substituent Effects in Parallel-Displaced π-π Stacking Interactions: Distance Matters, Angew. Chem. Int. Ed. 2017, **56,** 11252 –11257, DOI: 10.1002/anie.201703744).

18. V.G. Viju Kumar, V.G. Vidya, Crystal architecture, DFT and Hirshfeld surface analysis of novel 'double open-end spanner' type dimer derived from 4-aminoantipyrine, Journal of Molecular Structure 1270 (2022) 133882, https://doi.org/10.1016/j.molstruc.2022.133882.

19. Joshua J McKinnon, Mark A Spackman, Anthony S Mitchell, Novel tools for visualizing and exploring intermolecular interactions in molecular crystals, Acta Crystallogr B. 2004 Dec;60(Pt 6):627-68, Doi:10.1107/S0108768104020300.

20. Meenukutty, M. S., Mohan, A. P., Vidya, V. G., Viju Kumar, V. G. Synthesis, characterization, DFT analysis and docking studies of a novel Schiff base using 5-bromo salicylaldehyde and β-alanine. ***Heliyon***, e09600, **2022**. https://doi.org/10.1016/j.heliyon.2022.e09600